

# Interpretation of radio continuum and molecular line observations of Sgr B2: free-free and synchrotron emission, and implications for cosmic rays

R.J. Protheroe<sup>1\*</sup> J. Ott<sup>2,3†</sup> R.D. Ekers<sup>4</sup> D.I. Jones<sup>1,4</sup> R.M. Crocker<sup>5</sup>

<sup>1</sup>*Department of Physics, School of Chemistry & Physics, University of Adelaide, South Australia 5000, Australia.*

<sup>2</sup>*National Radio Astronomy Observatory, 520 Edgemont Road, Charlottesville, VA 22903, USA*

<sup>3</sup>*California Institute of Technology, 1200 E. California Blvd., Caltech Astronomy, 105-24, Pasadena, CA, 91125, USA.*

<sup>4</sup>*Australia Telescope National Facility, CSIRO, P.O. BOX 76 Epping, NSW 1710, Australia.*

<sup>5</sup>*J.L. William Fellow, School of Physics, Monash University, Victoria, Australia.*

Accepted . Received ; in original form .

## ABSTRACT

Recent ammonia (1,1) inversion line data on the Galactic star forming region Sgr B2 show that the column density is consistent with a radial Gaussian density profile with a standard deviation of 2.75 pc. Deriving a formula for the virial mass of spherical Gaussian clouds, we obtain  $M_{\text{vir}} = 1.9 \times 10^6 M_{\odot}$  for Sgr B2. For this matter distribution, a reasonable magnetic field and an impinging flux of cosmic rays of solar neighbourhood intensity, we predict the expected synchrotron emission from the Sgr B2 giant molecular cloud due to secondary electrons and positrons resulting from cosmic ray interactions, including effects of losses due to pion production collisions during diffusive propagation into the cloud complex.

We assemble radio continuum data at frequencies between 330 MHz and 230 GHz. From the spectral energy distribution the emission appears to be thermal at all frequencies. Before using these data to constrain the predicted synchrotron flux, we first model the spectrum as free-free emission from the known ultra compact HII regions plus emission from an envelope or wind with a radial density gradient, and obtain an excellent fit. We thus find the spectrum at all frequencies to be dominated by thermal emission, and this severely constrains the possible synchrotron emission by secondary electrons to quite low flux levels. The absence of a significant contribution by secondary electrons is almost certainly due to multi-GeV energy cosmic rays being unable to penetrate far into giant molecular clouds. This would also explain why 100 MeV–GeV gamma-rays (from neutral pion decay or bremsstrahlung by secondary electrons) were not observed from Sgr B2 by EGRET, while TeV energy gamma-rays were observed, being produced by higher energy cosmic rays which more readily penetrate giant molecular clouds.

**Key words:** cosmic rays, HII regions, radiation mechanisms: non-thermal, ISM: individual: Sgr B2 Giant Molecular Cloud, radio lines: ISM, radio continuum: ISM

## 1 INTRODUCTION

Molecular clouds have long been studied as laboratories for star formation. This has led to a wealth of information about the physical characteristics of clouds and their chemical makeup, usually obtained by observing emission/absorption lines of molecules such as CO, OH, etc., which reveal the presence of molecular gas. Most molecular cloud emission is

thermal, from the HII regions and/or dust emission. Cosmic rays play an important role in molecular cloud evolution by partially ionizing even the cold molecular gas, thereby affecting, through ambipolar diffusion, the dynamics of cloud collapse by coupling the magnetic field to the partially ionized gas. This in turn could result in amplification of the ambient magnetic field during cloud collapse, and give rise to the correlation found by Crutcher (1999) between average density of molecular gas of molecular clouds and their line-of-sight magnetic fields. From VLA observations of Zeeman splitting of the HI line Crutcher (1996) found a line of sight

\* E-mail: rprother@physics.adelaide.edu.au.

† currently a Jansky Fellow of the National Radio Astronomy Observatory

magnetic field for Sgr B2 of  $B_{LOS} \approx 0.5$  mG to apply to the outer envelope of the cloud complex, and this would suggest that the magnetic field amplitude could be even higher in the inner parts of the complex. In fact, both Lis & Goldsmith (1989) and Crutcher (1996) actually countenance average magnetic field strengths as high as  $\sim 2$  mG for the Sgr B2 cloud on the basis of the theoretical prejudice that the cloud be magnetically supported against gravitational collapse; we cannot exclude that such field strengths may actually apply on large scales in the complex.

Recent studies of the ionization rate by van der Tak et al. (2006) show that the cosmic ray ionization rate of dense molecular clouds in the Galactic Centre (GC) region may be as much as a factor  $\sim 10$  higher than in molecular clouds in the solar neighbourhood. Other evidence for a higher cosmic ray density in the GC region may come from the observation of 6.4 keV iron line emission. Assuming that low energy cosmic rays are responsible for heating the molecular gas, Yusef-Zadeh et al. (2007) estimated the energy densities of cosmic rays in GC molecular clouds to range from  $19 \text{ eV cm}^{-3}$  to  $6 \times 10^4 \text{ eV cm}^{-3}$ , with  $51 \text{ eV cm}^{-3}$  for Sgr B2. This is much higher than the energy density of cosmic rays in the solar neighbourhood which is  $\sim 1 \text{ eV cm}^{-3}$ . Since ionisation is most effective for low-energy cosmic ray nuclei, and because cosmic ray energy spectra typically have an inverse power-law form, it is the cosmic rays with kinetic energies much less than 1 GeV/nucleon that are mainly responsible. Hence the enhanced ionization in the GC region could be due to an overall enhancement of the cosmic ray flux there or to an additional, steep, low-energy component (Crocker et al. 2007).

High densities of low-energy hadronic cosmic ray nuclei within regions of dense gas will result in enhanced  $\sim 100$  MeV gamma-ray emission through enhanced pion production followed by  $\pi^0 \rightarrow \gamma\gamma$  decay and  $\pi^\pm \rightarrow \mu^\pm \rightarrow e^\pm$  decay followed by secondary electron bremsstrahlung. The High Energy Stereoscopic System (HESS) recently completed a survey of the Galactic Centre (Aharonian et al. 2006), and found a broad scale correlation between the  $\gamma$ -ray emission and column density of the molecular gas, but required the GC region cosmic ray flux at  $\sim 10$  TeV to be about 10 times higher than that observed in the solar neighbourhood. Such an enhancement in the GC cosmic ray flux at GeV energies was not inferred by EGRET observations of 100 MeV gamma-rays from the central region of the Galaxy, indeed, it was explicitly noted by Mayer-Hasselwander et al. (1998) that no localized excess associated with the Sgr B complex was detected by EGRET excluding the possibility of a significantly enhanced CR density in these clouds – *in the appropriate energy range*, of course. One possible explanation of this, and the high ionization rate inferred by van der Tak et al. (2006), that has been suggested by Crocker et al. (2007) is that in the Galactic Centre region there may be a steep component  $E^{-2.7}$  with a normalization at  $\sim 10$  GeV energies comparable to that locally in order to explain the EGRET result, and an even steeper lower energy component to explain the high ionization rate, and finally a flat  $E^{-2.2}$  component negligible at GeV energies but giving a tenfold increase at  $\sim 10$  TeV to explain the HESS data. Such a flat component may arise as suggested by Cheng et al. (2007) if periodic acceleration at Sgr A\* occurs when stars are

tidally disrupted at a rate of  $10^{-5} \text{ year}^{-1}$ , and diffuse at a distance of  $\sim 500$  pc before  $pp$  losses steepen the spectrum on a timescale of  $\sim 10^4$  years. However, to also explain the broadband radio to gamma ray spectral energy distribution of the Sgr B region, with hadronic models they need a rather strong average magnetic field, viz., 2.2-3.7 mG.

The same interactions of cosmic ray nuclei within regions of dense gas which may lead to enhanced gamma-ray production (at least at TeV energies) should produce copious secondary electrons and positrons which may in turn produce synchrotron emission in GMC magnetic fields which are observed to be higher than elsewhere in the interstellar medium. This possibility was the motivation for the present work as well as recent observations at 1.4 GHz and 2.4 GHz of the Sgr B2 GMC (Jones et al. 2008a), and of the dense cold starless cores G333.125-0.562 and IRAS 15596-5301 (Jones et al. 2008b). The dense cores were chosen because, unlike Sgr B2, they are well away from the central region of the Galaxy and would have a cosmic ray environment expected to be similar to that of the Solar region. They are of much lower mass than the Sgr B2 GMC, and their magnetic fields are unknown. The non-detection of these dense cold starless cores in non-thermal emission was used to place upper limits on the magnetic fields of both of  $\sim 0.5$  mG.

Here, we investigate whether one should expect to see radio synchrotron emission by secondary  $e^\pm$  from giant molecular cloud (GMC) complexes. We shall compare our predictions of the expected synchrotron emission with our recent observations (Jones et al. 2008a) to draw conclusions about the cosmic ray environment around and within the Sgr B2 GMC. We chose the Sgr B2 GMC for this study because of its large mass, its location in the central region of the Galaxy where the cosmic ray density may be higher than that in the solar neighbourhood, and its high magnetic field. This was in spite of being aware of its complicated nature, and the likely difficulty in disentangling non-thermal from thermal emission in this source – our search for any comparable molecular cloud with no star formation in the central region of the Galaxy was unsuccessful.

## 2 SGR B2 CLOUD COMPLEX: MASS AND DENSITY

The combination of magnetic fields and secondary  $e^\pm$  (and also primary  $e^-$ ) will lead to the emission of synchrotron radiation from molecular clouds which, because of its relatively steep spectrum, may show up at frequencies below which the free-free emission from HII regions turns down after becoming optically thick. The observed flux of cosmic ray  $e^\pm$  contains at least  $\sim 15\%$  positrons at 10 GeV (Grimani et al. 2002; Beatty, et al. 2004). Given that secondary electrons and positrons would be produced *in situ* inside molecular clouds by cosmic ray nuclei, they should be sites of copious secondary  $e^\pm$  production. Since the production of these secondaries is proportional to the product of the matter and cosmic ray densities within the clouds, there should be an appreciable flux of synchrotron radiation at low frequencies from molecular clouds due to secondary electrons, provided cosmic rays can penetrate the clouds.

Sgr B2 is one of the largest and most complex molecular cloud/HII regions in the Galaxy – see Lang et al. (2008)

for a discussion and review of the continuum emission measurements. It lies near the Galactic Centre, and we assume it to be  $\sim 8.5$  kpc from Earth, at a projected distance of 100 pc from the Galactic Centre. Sgr B2 comprises at least four components (Gordon et al. 1993). These are three dense cores Sgr B2(N), (M) and (S) and a less dense outer envelope (OE). The dense cores are sites of massive star formation and have HII regions, ultra-compact HII regions (UCHII) – Gaume & Claussen (1990) have found more than 60 UCHII sources in Sgr B2(M) alone. X-ray sources associated with HII regions, X-ray sources with no radio or IR counterparts (Takagi, Murakami & Koyama 2002), dense cores, embedded protostars and molecular masers (Goicoechea 2004) are also found. The cores are small ( $\sim 0.5$  pc), warm ( $\approx 45$ – $60$ K), light ( $10^3$ – $10^4 M_\odot$ ), dense ( $10^{6-7} \text{ cm}^{-3}$ ), and correspond to  $\sim 5\%$  of the cloud mass. On the other hand, the envelope is cool ( $\sim 10$  K), massive ( $7.6 \times 10^5 M_\odot$ ), and less dense ( $10^5 \text{ cm}^{-3}$ ). It is thought that at wavelengths  $\lambda > 3\text{mm}$  (100 GHz), free-free emission dominates, whilst at shorter wavelengths thermal emission from dust dominates (Gordon et al. 1993).

There have also been radio continuum, X-ray, and recently, as we mentioned earlier,  $\gamma$ -ray observations of the Galactic Centre. The large-scale diffuse radio emission from the GC region has been observed at 330MHz extensively using the VLA (La Rosa et al. (2005) and references therein). It has also been observed in hard X-rays by INTEGRAL (Neronov et al. 2005). There have also been *Chandra* and ASCA X-ray observations of the Galactic Centre, where the authors argue for a reflection nebula of Compton scattered X-rays from the Galactic Centre source Sgr A\* at an earlier time (Murakami et al. 2000; Takagi, Murakami & Koyama 2002; Murakami et al. 2001; Fryer et al. 2006).

Recently, Ott et al. (2006) have observed the ammonia (1,1) inversion line over the Sgr B2 complex and the resulting zeroth moment map (image of the intensity integrated over the line) is shown in Fig. 1. The data, obtained with the Australia Telescope Compact Array (ATCA), show the Sgr B2 parent molecular cloud in sharp contrast against the surrounding molecular material. This is mainly due to the property of an interferometer to filter out very extended structures. Excluding the absorption of the ammonia (1,1) line by the prominent HII regions Sgr B2(M) and Sgr B2(N), we find that the intensity integrated over the line varies with position in such a way that the column density profile is consistent with a two-dimensional Gaussian with a standard deviation of  $\sigma = 2.75 \pm 0.1$  pc (assuming a distance of 8.5 kpc) centred midway between Sgr B2(N) and Sgr B2(M) (see Fig. 2).

For optically thin emission, the intensity integrated over the ammonia (1,1) line is proportional to the column density of ammonia provided the temperature is constant, and so to that of molecular hydrogen

$$\int_{(1,1)\text{line}} I_\nu d\nu \propto N_{\text{NH}_3} \propto N_{\text{H}_2},$$

where the final proportionality also assumes the fractional  $\text{NH}_3$  abundance is constant. For the assumptions above, this implies that the volume density profile for  $\text{H}_2$  must be a radial Gaussian density profile, too. For the case of a cloud with spherical symmetry, if the column density is a two-dimensional Gaussian surface density, then the volume den-

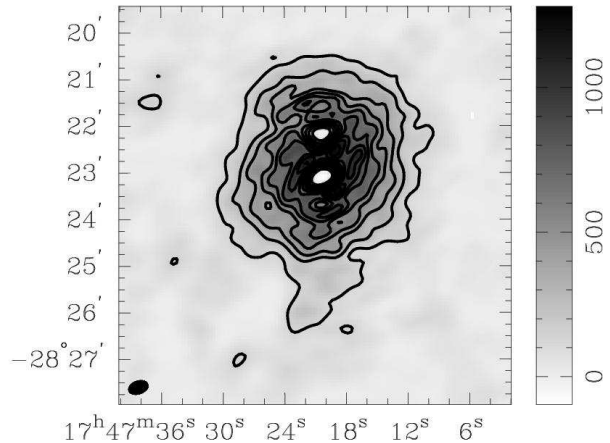


**Figure 1.** Image and contours showing the zeroth moment of the (1,1) line of  $\text{NH}_3$  for the region around Sgr B2. J2000 coordinates are used. Contours from 10% peak intensity until 90% peak intensity in increments of 10%. Note that around the Sgr B2(M) and Sgr B2(N) HII regions, the  $\text{NH}_3$  line emission is strongly attenuated due to thermal bremsstrahlung absorption. The beam is located in the lower left-hand corner of the image, and is  $26 \times 17''$  at a position angle of  $-70^\circ$ . The intensity scale, located on the right of the image is from  $-96$  to  $1280 \text{ K km s}^{-1}$ .

sity must be described by a three-dimensional Gaussian with the same standard deviation,

$$n_{\text{H}_2}(\vec{r}) = \frac{M_{\text{H}_2}}{2m_{\text{H}}} \frac{1}{(\sqrt{2\pi}\sigma)^3} e^{-(x^2+y^2+z^2)/(2\sigma^2)}$$

in which case the column density at impact parameter  $b$  from the cloud centre is

$$N_{\text{H}_2}(b) = \frac{M_{\text{H}_2}}{2m_{\text{H}}} \frac{1}{2\pi\sigma^2} e^{-b^2/(2\sigma^2)}.$$

Of course, the column density averages over density variations along the line of sight, and so the smooth radial Gaussian density profile will be an approximation to the true density distribution. Indeed, the cloud structure typically is fractal and the mass distribution follows a power law, and the column density contains contributions from a good number of individual cloudlets.

## 2.1 Virial mass of a Gaussian spherical cloud

Here we derive, for the first time, the virial mass of a cloud complex with a radial Gaussian density profile. If a cloud is thermally supported, its kinetic energy is

$$K = \frac{3}{2} \frac{M}{\langle \mu \rangle m_u} kT$$

where  $\langle \mu \rangle$  is the mean atomic mass,  $m_u$  is the unified atomic mass unit,  $k$  Boltzmann constant and  $T$  the temperature. The mass inside radius  $r$  of a Gaussian spherical cloud is

$$\begin{aligned} M(< r) &= M \frac{2}{\sqrt{\pi}} \int_0^{r^2/2\sigma^2} x^{1/2} e^{-x} dx \\ &= M \frac{2}{\sqrt{\pi}} \Gamma(3/2, r^2/2\sigma^2). \end{aligned}$$

where  $\Gamma(a, x)$  is the incomplete Gamma function. The gravitational potential energy of a Gaussian spherical cloud is

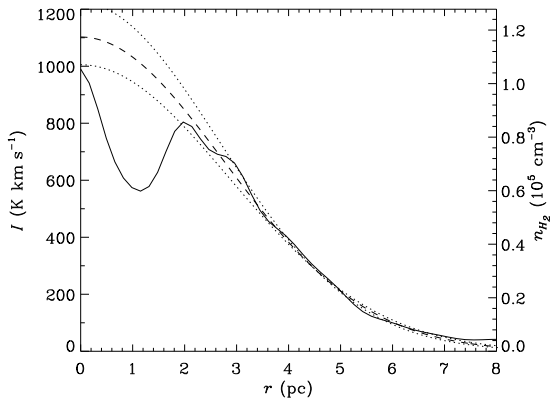


**Figure 2.** Azimuthally averaged intensity of the (1,1) inversion line of  $\text{NH}_3$  vs. impact parameter from the centre of Sgr B2 assuming a distance of 8.5 kpc. The thick dashed line is a Gaussian fit to the data between 2 pc and 7 pc with  $\sigma=2.75$  pc; at impact parameters less than 2 pc the data are affected by absorption effects against Sgr B2 (N) and (M), and beyond 7 pc the intensity may be emission from a southern cloud possibly unrelated to the Sgr B2 cloud (cf. Fig. 1). This fit provides the extrapolation of the profile toward the centre; the thin dotted lines give fits having  $\sigma=2.65$  and 2.85 pc and are shown to give an indication of the uncertainty in  $\sigma$ . The right hand axis shows the inferred density as a function of radius for the  $\sigma=2.75$  pc fit.

then

$$U = - \int_0^\infty GM \frac{2}{\sqrt{\pi}} \Gamma(3/2, r^2/2\sigma^2) \frac{4\pi r^2 \rho(r)}{r} dr$$

$$= - \frac{GM^2}{2\sqrt{\pi}\sigma}.$$

Usually the temperature is obtained from observed thermal Doppler broadening of a narrow line of some element or molecule with atomic mass  $\mu$ . Then, if the emission is optically thin, the line has a Gaussian profile with standard deviation (measured in m/s) of

$$\sigma_v = \sqrt{\frac{kT}{\mu m_u}}$$

giving

$$\frac{kT}{m_u} = \mu \sigma_v^2.$$

From the virial theorem,  $K = -\frac{1}{2}U$ , we obtain

$$M_{\text{vir}} = \frac{6\sqrt{\pi}\sigma}{G} \frac{\mu}{\langle\mu\rangle} \sigma_v^2.$$

Putting this in practical units, we obtain

$$\frac{M_{\text{vir}}}{M_\odot} = 444 \frac{\mu}{\langle\mu\rangle} \left( \frac{\sigma}{1 \text{ pc}} \right) \left( \frac{v_{\text{FWHM}}}{1 \text{ km s}^{-1}} \right)^2.$$

This is a factor 2.1 higher than the usual formula for a uniform density sphere of radius  $R = \sigma$ .

If the cloud is supported solely by turbulent motion, as is certainly the case for GMCs, the line width is determined by the RMS turbulent velocity rather than the thermal RMS speed of the molecular species being observed, and then the

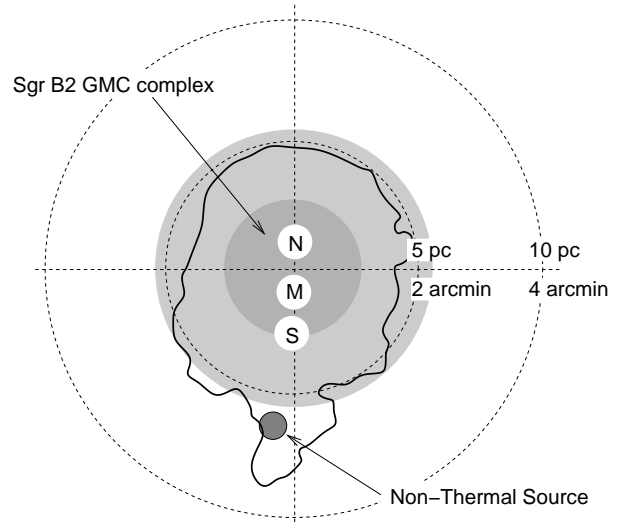


**Figure 3.** Sketch of the morphology of Sgr B2 showing the locations of the prominent HII regions, the  $200 \text{ K km s}^{-1}$   $\text{NH}_3$  contour, and the locations of the main Sgr B2 cloud complex (shaded regions have radius equal to one and two standard deviations of the assumed radial Gaussian density profile). The strong southern non-thermal source indicated is excluded from the present analysis.

virial mass is given by

$$\frac{M_{\text{vir}}}{M_\odot} = 444 \left( \frac{\sigma}{1 \text{ pc}} \right) \left( \frac{v_{\text{FWHM}}}{1 \text{ km s}^{-1}} \right)^2. \quad (1)$$

## 2.2 Mass of Sgr B2 cloud complex

The velocity FWHM of the ammonia (1,1) line observations of Sgr B2 is  $39.7 \text{ km s}^{-1}$ , implying the cloud is supported by turbulence rather than being thermally supported. The virial mass of Sgr B2 based on Eq. 1 and  $\sigma=2.75\pm 0.1$  pc is  $M_{\text{vir}} = (1.9\pm 0.1) \times 10^6 M_\odot$ . Since the virial mass of a cloud complex with a radial Gaussian density profile is a factor 2.1 higher than that of a uniform density sphere, we suggest that the typical uncertainty in mass determinations using the virial theorem arising from uncertainty in cloud structure could be as large as a factor  $\sim 2$ . Sato (2000) gives a mass of  $(1-2) \times 10^6 M_\odot$  for Sgr B2(M) assuming a radius of 1.5 pc, and in the HESS paper on the GC region Aharonian et al. (2006) give a total mass of  $(6-15) \times 10^6 M_\odot$  for a  $0.5^\circ \times 0.5^\circ = 75 \text{ pc} \times 75 \text{ pc}$  region surrounding Sgr B2 based on CS data (Tsuboi 1999).

Taking the virial mass of  $(1.9 \pm 0.1) \times 10^6 M_\odot$  to be the mass of molecular gas (assumed to be almost entirely  $\text{H}_2$ ) in the Sgr B2 cloud complex, and a radial Gaussian density profile with a standard deviation of  $\sigma=2.75\pm 0.1$  pc, the maximum column density is  $N_{\text{H}_2} = (2.5 \pm 0.1) \times 10^{24} \text{ cm}^{-2}$ . The density is  $n_{\text{H}_2} = (1.2 \pm 0.1) \times 10^5 \text{ cm}^{-3}$  at the centre of the Sgr B2 complex, and decreases to  $10 \text{ cm}^{-3}$  at a radius of  $\sim 12$  pc which we shall consider to be its outer radius. The  $\text{H}_2$  number density (dotted curve) may be read off the right-hand axis in Figure 2. A sketch of the Sgr B2 region showing the ammonia (1,1) line 10% contour level of the zeroth moment map, the (N), (S) and (M) HII regions,

and the size of inferred Gaussian cloud complex is given in Figure 3.

### 3 COSMIC RAY SECONDARY ELECTRON PRODUCTION

The Galactic synchrotron emission is due to accelerated (primary) cosmic ray electrons, and to electrons and positrons produced as secondaries. The production rate of secondary electrons and positrons depends only on the spectrum and intensity of cosmic ray nuclei, and the density of the interstellar matter. We use the production rate of electrons and positrons  $q_m(E)$ , per solar mass of interstellar matter per unit energy ( $M_\odot^{-1} \text{ GeV}^{-1} \text{ s}^{-1}$ ), for the cosmic ray spectrum and composition observed above the Earth's atmosphere based on figure 4 of Moskalenko & Strong (1998).

The production of large numbers of positrons can be traced through their 511 keV annihilation line, and this has been observed by INTEGRAL from within  $8^\circ$  of the Galactic Centre region (Weidenspointner 2006). To explain these observations, Beacom & Yüksel (2006) show that the production of positrons is  $\sim 10^{50}$  per year in the central region of the Galaxy, and that they must be injected at energies below  $\sim 3$  MeV to avoid excessive gamma ray emission at higher energies (excluding the possibility that they are supplied by the  $pp \rightarrow \pi^+ \rightarrow e^+$  chain).

The production spectrum of secondary cosmic ray  $e^\pm$  has a gradual cut-off below  $\sim 0.3$  GeV due to threshold for  $\pi^\pm$  in  $p-p$  collisions. Nevertheless we should check that their production rate in molecular clouds does not exceed the stringent constraint on production of  $\sim 10^{50}$  positrons per year. Assuming the cosmic ray spectrum in the Galactic Centre region has the same shape there as locally, but is enhanced by a factor  $f_{CR}$ , we find the total production rate of secondary  $e^+$  in Sgr B2 alone to be  $1.9 \times 10^6 M_\odot f_{CR} \int q_m(E) dE = 7.8 \times 10^{45} f_{CR} e^+$ /year. This certainly does not exceed the limit for  $f_{CR}$  in the range 1–10 which seems reasonable based on EGRET and HESS gamma-ray data, and taking account of the likelihood that cosmic rays may not fully penetrate clouds the production rate is probably less. Indeed, one would require  $\sim 3 \times 10^{11} M_\odot / f_{CR}$  of interstellar gas within 1 kpc of the Galactic Centre to exceed the observed  $e^+$  production rate.

We shall delay until later in this section a discussion of the complex problem of penetration of Galactic cosmic ray nuclei and electrons into molecular clouds. For the moment, then, we shall assume that Galactic cosmic rays freely penetrate the cloud and that their spectrum inside the cloud complex is the same as that in the solar neighbourhood. The production spectrum of electrons and positrons per unit volume per unit energy ( $e^\pm \text{ cm}^{-3} \text{ GeV}^{-1} \text{ s}^{-1}$ ) at position  $\vec{r}$  in the Galactic Centre region is then the product of the density of interstellar gas at position  $\vec{r}$  multiplied by the production rate per unit mass

$$q(E, \vec{r}) = f_{CR} n_{H_2}(\vec{r}) q_m(E) 2m_H / M_\odot. \quad (2)$$

For moderate molecular cloud densities  $n_H > 10^2 \text{ cm}^{-3}$  and magnetic fields  $B > 10^{-5} \text{ G}$ , the relatively short energy loss times appear to justify neglecting diffusive transport of electrons – we shall discuss this point in detail in a later section. Then one readily obtains, by numerical integration,

the ambient number density of electrons and positrons, per unit energy,  $n^\pm(E, r) (e^\pm \text{ cm}^{-3} \text{ GeV}^{-1})$ , at various positions  $\vec{r}$  within the molecular cloud complex:

$$n(E, \vec{r}) = \frac{\int_E^\infty q(E, \vec{r}) dE}{dE/dt},$$

where  $dE/dt$  is the total rate of energy loss of electrons at energy  $E$  due to ionization, bremsstrahlung and synchrotron emission (because of the energies involved, we neglect positron annihilation, and assume electrons and positrons suffer identical energy losses). Electrons lose energy by ionization losses in neutral molecular hydrogen at a rate (in  $\text{GeV s}^{-1}$ ) of

$$\frac{dE}{dt}_{\text{ioniz}} = 5.5 \times 10^{-17} \left( \frac{n_{H_2}}{1 \text{ cm}^{-3}} \right) \times (\ln \gamma + 6.85)$$

and by bremsstrahlung at a rate (in  $\text{GeV s}^{-1}$ ) of

$$\frac{dE}{dt}_{\text{bremss}} = 1.5 \times 10^{-15} \left( \frac{E}{1 \text{ GeV}} \right) \times \left( \frac{n_{H_2}}{1 \text{ cm}^{-3}} \right).$$

The synchrotron energy loss rate (in  $\text{GeV s}^{-1}$ ) is

$$\frac{dE}{dt}_{\text{synch}} = 1.0 \times 10^{-12} \times \left( \frac{B_\perp}{1 \text{ gauss}} \right)^2 \times \gamma^2$$

where  $B_\perp$  is the component of magnetic field perpendicular to the electron's direction. For an isotropic electron population the solid-angle average is  $\langle B_\perp \rangle = \pi B/4$ , and, assuming the magnetic field can be in any direction with respect to the line of sight, an appropriate value for the line-of-sight component of magnetic field obtained from Zeeman splitting  $B_{LOS}$  would be  $\langle B_{LOS} \rangle = B/2$ . Hence taking  $B_\perp = \pi B_{LOS}/2$  is reasonable. Given the observed value is  $B_{LOS} = 0.5 \text{ mG}$  (Crutcher 1996), we adopt  $B_\perp = 0.8 \text{ mG}$ .

The synchrotron emission is calculated using standard formulae in synchrotron radiation theory (Rybicki & Lightman 1979)

$$\begin{aligned} j_\nu &= \frac{\sqrt{3} e^3}{4\pi m_e c^2} \left( \frac{B_\perp}{1 \text{ gauss}} \right) \times \int_{m_e c^2}^\infty F(\nu/\nu_c) n(E, \vec{r}) dE \\ &\quad \text{erg cm}^{-3} \text{ s}^{-1} \text{ sr}^{-1} \text{ Hz}^{-1}, \\ \nu_c &= 4.19 \times 10^6 (E/m_e c^2)^2 \left( \frac{B_\perp}{1 \text{ gauss}} \right) \text{ Hz}, \\ e &= 4.8 \times 10^{-10} \text{ esu}, \\ m_e c^2 &= 8.18 \times 10^{-7} \text{ erg}, \\ F(x) &= x \int_x^\infty K_{\frac{5}{3}}(\xi) d\xi. \end{aligned}$$

and  $K_{\frac{5}{3}}(x)$  is the modified Bessel function of order 5/3.

The Razin effect reduces non-thermal emission at low frequencies by suppression of synchrotron emission at  $\nu < \gamma_e \nu_p$  where  $\nu_p$  is the plasma frequency and  $\gamma_e$  is the Lorentz factor of the radiating electrons, and the effect is negligible where  $\nu \gg 20n_e/B$  where  $n_e$  is the number density of free electrons ( $\text{cm}^{-3}$ ) and  $B$  is in Gauss. For the Sgr B2 cloud assuming  $B_\perp = 0.8 \text{ mG}$  and our lowest frequency of interest being 330 MHz, the Razin effect will be small if  $n_e \ll 10^5 \text{ cm}^{-3}$ . Given that in a molecular cloud  $n_e \ll n_{H_2}$  and for the Sgr B2 main complex we estimate the central density to be  $n_{H_2} = 1.2 \times 10^5 \text{ cm}^{-3}$ , we can safely neglect the Razin effect in the present work.

For a perpendicular component of magnetic field of

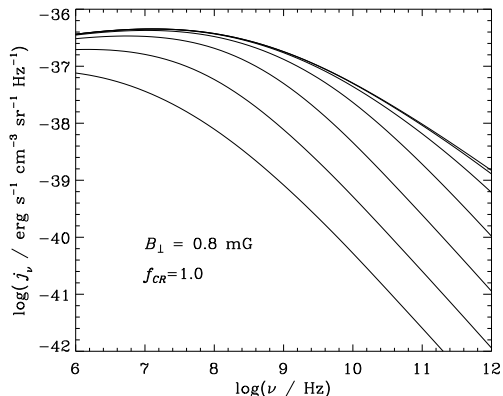


**Figure 4.** Synchrotron emission coefficient of secondary electrons produced by cosmic ray interactions for densities  $n_{H_2} = 10^0$  (bottom curve),  $10^1$ ,  $10^2$ ,  $\dots$ ,  $10^6$   $\text{cm}^{-3}$  (top curve).

0.8 mG, as may be appropriate for Sgr B2, and the solar neighbourhood cosmic ray spectrum, we find the specific emission coefficient due to synchrotron emission by secondary electrons as shown in Fig. 4 for various gas densities. Note that for higher density regions, electron energy loss by bremsstrahlung dominates over synchrotron losses reducing the synchrotron power per unit mass relative to lower density regions. As can be seen, this has the effect that at low frequencies the synchrotron emission coefficient becomes almost independent of density for  $n_{H_2} > 10^3$   $\text{cm}^{-3}$  and mG fields.

### 3.1 Penetration of Cosmic Ray Nuclei into the Sgr B2 Cloud Complex

Work on this subject has been motivated mainly by gamma-ray observations, particularly of the central region of the Galaxy. An important contribution to the Galactic gamma-ray intensity comes from interactions of cosmic ray nuclei through pion production and subsequent decay  $\pi^0 \rightarrow \gamma\gamma$ , and  $\pi^\pm \rightarrow \mu^\pm \rightarrow e^\pm$  followed by bremsstrahlung or inverse Compton. Of course primary accelerated electrons are also important for the latter two processes. Put simply, if cosmic rays can freely enter molecular clouds then the gamma-ray flux will be higher than if they cannot. In the present work we are interested in synchrotron radiation by the same secondary  $e^\pm$ . Another motivation has been to estimate the ionization rate due to cosmic rays. Again, this depends crucially on the extent of penetration of cosmic rays responsible for ionization, mainly those of lower energy.

The nature and extent of penetration of cosmic rays into molecular clouds has is not yet fully understood, and has a long history. Skilling & Strong (1976) concluded that the very low energy cosmic rays mainly responsible for ionization of cloud material are efficiently excluded from clouds, whereas Cesarsky & Volk (1978) concluded that molecular clouds are pervaded by inter-cloud cosmic rays. Dogel' & Sharov (1990) considered acceleration of charged particles by turbulence in giant molecular clouds, and suggested that this mechanism may explain the unidentified gamma-ray sources discovered by COS-B, and estimated the

synchrotron radio emission of accelerated primary and secondary electrons in molecular clouds in this scenario.

Certainly, at multi-TeV energies there should be no problem in cloud penetration, and this was recently confirmed by the excellent correlation between TeV gamma-ray intensity as measured by HESS (Aharonian et al. 2006) and the column density of molecular gas for the Galactic Centre region. At lower energies, the interpretation of the 100 MeV–GeV energy gamma ray intensity measured by EGRET (Mayer-Hasselwander et al. 1998) toward the Galactic Centre region is ambiguous and we await with great interest the higher resolution data from GLAST due for launch in 2008. In this context, Gabici et al. (2007) have recently investigated the penetration of cosmic rays into molecular clouds to understand the importance of this for gamma ray emission at GeV and TeV energies. They considered proton-proton collision losses as cosmic rays diffuse into a cloud. Taking a typical cloud to have  $n_{H_2} = 300$   $\text{cm}^{-3}$ ,  $B = 10$   $\mu\text{G}$  and radius 20 pc, they found that, for a diffusion coefficient based on that which seems to apply to cosmic rays throughout the Galaxy (as determined by secondary to primary composition measurements), cosmic rays would freely penetrate. They also found, however, that if the diffusion coefficient inside the cloud is smaller, say 0.01 of the average Galactic one, that exclusion becomes relevant for 10–100 GeV cosmic ray nuclei resulting in suppression of GeV gamma-ray emission. Given that the Sgr B2 complex has a much higher density and magnetic field than that modelled by Gabici et al. (2007), it is clearly necessary to determine the extent of suppression of  $e^\pm$  production.

Cosmic ray protons and nuclei produced outside the cloud will penetrate the cloud by diffusion and advection, and lose typically half their energy in  $pp$  collisions on a time scale  $t_{pp} \approx 5 \times 10^7 n_{H_2}^{-1}$  yr, where  $n_{H_2}$  is in  $\text{cm}^{-3}$ . The advection timescale is  $t_{adv} \equiv R_{\text{cloud}}/\sigma_v$  which for  $R_{\text{cloud}} = 12$  pc and  $\sigma_v = 39.7$   $\text{km s}^{-1}$  is  $t_{adv} \approx 3 \times 10^5$  years.

The diffusion timescale is

$$t_{\text{diff}}(E) \equiv \frac{R_{\text{cloud}}^2}{2D(E)} \quad (3)$$

where  $D(E)$  is the diffusion coefficient, which depends on the ambient magnetic field and the spectrum of turbulence. The minimum diffusion coefficient for a completely tangled magnetic field is the so-called ‘‘Bohm diffusion coefficient’’ which, for relativistic protons, is  $D_{\text{min}}(E) = \frac{1}{3} r_g(E) c \propto E$  where  $r_g \approx 10^{-9} E_{\text{GeV}} B_{\text{mG}}^{-1}$  pc is the gyroradius,  $B_{\text{mG}}$  is the magnetic field in milligauss and  $E_{\text{GeV}}$  is the proton energy in GeV. Models of cosmic ray propagation in the Galaxy which are consistent with the observed relative abundance of ‘‘primary’’ cosmic ray nuclei (e.g. Carbon) and ‘‘secondary’’ cosmic ray nuclei (e.g. Boron) – the latter produced by spallation of primary cosmic ray nuclei – suggest that  $D(E) \propto E^\alpha$  where  $\alpha \sim 0.3 - 0.7$ . If a Kolmogorov spectrum of turbulence is present, then one would expect  $\alpha = 1/3$ , but in the presence of strong magnetic fields a Kraichnan spectrum may give rise to  $\alpha = 1/2$ . Following Gabici et al. (2007), we adopt a diffusion coefficient

$$D(E) = 3 \times 10^{27} \chi \left[ \frac{E/(1 \text{ GeV})}{B/(3 \mu\text{G})} \right]^{0.5} \text{cm}^2 \text{s}^{-1} \quad (4)$$

where  $\chi \leq 1$  is a factor to account for the possible suppression (slowing) of diffusive transport.

Adopting a magnetic field of  $\sim 0.8$  mG, the typical energies of electrons or positrons responsible for synchrotron emission at 330 MHz - 1 GHz are  $\sim 0.3$ - $0.4$  GeV. Taking the primary proton energy to be  $\sim 10$  times higher, and setting the outer boundary of the Sgr B2 cloud to be  $\sim 12$  pc, this gives a diffusion timescale of  $\sim 10^4 \chi^{-1}$  yr. Comparing this diffusion time-scale with the loss timescale of only 500 years, for  $pp$  collisions in a central density of  $n_{H_2} \sim 10^5 \text{ cm}^{-3}$ , shows that, for the 0.8 mG magnetic field, penetration to the centre of the GMC complex is very improbable below  $\sim 3$  GeV energies. As we have already noted, because bremsstrahlung losses dominate in dense regions much of the synchrotron emission is expected to come from outer regions of Sgr B2, and it is penetration to these outer regions that matters most. For these regions the distance is obviously smaller and the density lower, suggesting that penetration of the outer region of the GMC complex is less of a problem.

We can make a more quantitative approximation of cosmic ray nucleus penetration by analogy with scattering ('s') and absorption ('a') of radiation and we define an effective optical thickness  $\tau_* = \tau_a(\tau_a + \tau_s)$  analogous to that used when considering radiative diffusion – see, e.g., Rybicki & Lightman (1979). In our case, for penetration from an outer boundary  $R$  to distance  $r$  from the centre we have

$$\tau_a(r) \approx \int_r^R 0.5[2n_{H_2}(r')] \sigma_{pp} dr' \quad (5)$$

where  $\sigma_{pp}(E) \approx 35$  mb above threshold, and the 0.5 factor is approximately the mean inelasticity (fractional energy lost) in  $pp$  collisions, and

$$\tau_s(E, r) \approx \int_r^R \frac{c}{3D(E, r')} dr' \quad (6)$$

since for isotropic diffusion, the effective mean free path is  $3D/c$ . Then the cosmic ray intensity at radius  $r$  is  $I_{CR} \approx e^{-\tau_*(E, r)} I_{CR}(E, R)$ .

The mean primary proton energy for a given secondary electron energy is given by

$$\langle E_p \rangle = \frac{\int E_p n_p(E_p) Y(E_e; E_p) dE_p}{\int n_p(E_p) Y(E_e; E_p) dE_p}$$

where  $n_p(E_p) dE_p$  ( $\text{cm}^{-3} \text{ GeV}^{-1}$ ) is the number density and of cosmic ray protons with energy  $E_p$  to  $(E_p + dE_p)$ , and  $Y(E_e; E_p) dE_{e\pm}$  ( $\text{g}^{-1} \text{ cm}^2$ ) are particle yields giving the rate of production of secondary electrons and positrons with energy  $E_e$  to  $(E_e + dE_e)$  per unit pathlength (in  $\text{g cm}^{-2}$ ) by a single cosmic proton of energy  $E_p$ . These particle yields can be obtained from accelerator data on charged pion production in  $pp$  collisions taking account of  $\pi \rightarrow \mu \rightarrow e$  decays (we use data kindly provided by T. Stanev, private communication). We find that for the local cosmic ray spectrum the mean primary proton total energy is

$$\langle E_p \rangle \approx 0.015 \gamma_e + 22 \gamma_e^{-0.5} \text{ GeV}. \quad (7)$$

So for observations made at frequency  $\nu$ , the appropriate cosmic ray proton energy to use is determined by assuming electrons radiate at the critical frequency, i.e. putting

$$\gamma_e = \left( \frac{\nu}{4.19 \times 10^6 B_\perp} \right)^{1/2} \quad (8)$$

into Eq. 7, where  $\nu$  is in Hz,  $B_\perp$  in gauss.

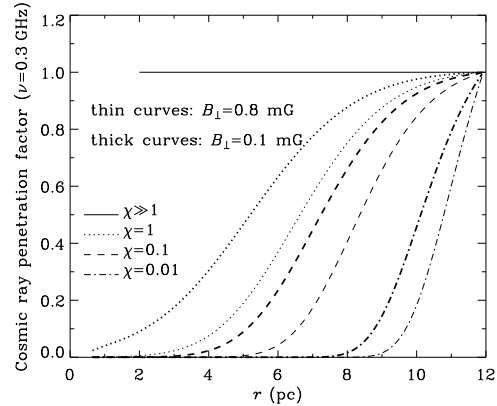


**Figure 5.** The cosmic ray penetration factor  $e^{-\tau_*[E_p(\nu, r)]}$  appropriate to  $\nu=0.3$  GHz is plotted against radius for the diffusion coefficient defined by Eq 4 with magnetic field and  $\chi$  as labeled ( $\chi \gg 1$  corresponds to unimpeded penetration).

The penetration factor  $e^{-\tau_*(E, r)}$  appropriate to an observing frequency of 0.3 GHz is plotted against radius from the centre of the Sgr B2 GMC for various values of the diffusive transport suppression factor  $\chi$  in Fig. 5 for  $B_\perp=0.8$  mG. To show how our results depend on assumed magnetic field, here and elsewhere in this paper we shall also show results for a lower magnetic field, arbitrarily chosen to be  $B_\perp=0.1$  mG. The penetration factor for this magnetic field is also shown in Fig. 5.

### 3.2 Diffusion of Secondary and Primary Cosmic Ray Electrons in the Sgr B2 Cloud Complex

Before predicting the synchrotron emission from the Sgr B2 GMC, we consider the diffusion of secondary  $e^\pm$  and primary cosmic ray  $e^-$ . Due to the high magnetic field, and high densities within the inner part of the GMC, electrons will suffer rapid energy losses there and this will limit how far they can propagate by diffusion. An estimate of how far an electron with Lorentz factor  $\gamma_e$  can propagate by diffusion before losing a significant fraction of its energy is given by what we shall refer to as the “diffusion-loss distance”

$$x_{\text{diff}}^e(\gamma_e) = \left[ \frac{D(\gamma_e m_e c^2) \gamma_e}{(d\gamma_e/dt)_{\text{total}}} \right]^{1/2}. \quad (9)$$

We plot  $x_{\text{diff}}^e(\gamma_e)$  for  $B_\perp=0.8$  mG and  $\chi=1$  in Fig. 6, and also for  $B_\perp=0.1$  mG to show the effect of a significantly lower magnetic field than appears to be present over the Sgr B2 GMC. For lower  $\chi$  values, the diffusion-loss distance is lower and is obtained by multiplying by  $\sqrt{\chi}$ .

For synchrotron radiation at the adopted magnetic field,  $B_\perp=0.8$  mG, the Lorentz factor of electrons mainly responsible for emission at 1 GHz is  $\gamma_e \approx 550$ . Near the centre of the GMC where  $n_{H_2} \sim 10^5 \text{ cm}^{-3}$  the diffusion loss distance is  $x_{\text{diff}}^e(550) \sim 0.2$  pc, at  $r=6$  pc where  $n_{H_2} \sim 10^4 \text{ cm}^{-3}$  we find  $x_{\text{diff}}^e(550) \sim 0.5$  pc, at  $r=8$  pc where  $n_{H_2} \sim 2 \times 10^3 \text{ cm}^{-3}$  we find  $\sim 1.3$  pc, and at  $r=12$  pc where  $n_{H_2} \sim 10 \text{ cm}^{-3}$  we find  $x_{\text{diff}}^e(550) \sim 3.7$  pc. From this we can draw the following conclusions: (a) at all distances the diffusion loss distance of electrons producing synchrotron radiation at 1 GHz is small compared to the radial coordinate and so we may safely

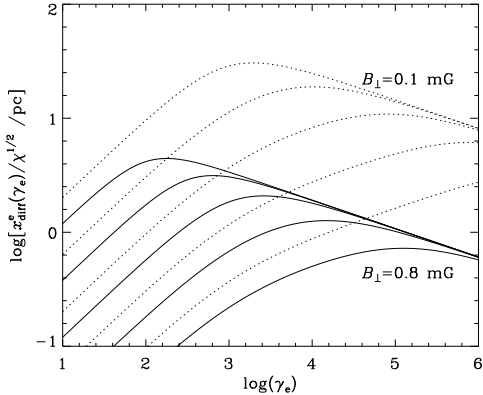


**Figure 6.** The diffusion-loss distance as defined by Eq. 9 plotted vs.  $\gamma_e$  for the diffusion coefficient given by Eq 4 for two magnetic fields (as labelled) and  $n_{H_2}=10^5 \text{ cm}^{-3}$  (bottom curves),  $10^4 \text{ cm}^{-3} \dots 10^1 \text{ cm}^{-3}$  (top curves).

make the approximation that secondary electrons within the GMC radiate where they are produced; (b) primary cosmic ray electrons from outside the GMC will not be able to propagate significantly towards the centre of the GMC and so are effectively excluded from the GMC complex. These conclusions are made even stronger if  $\chi < 1$ . However, primary electrons accelerated inside the GMC, e.g. by diffusive shock acceleration at supernova shocks or wind shocks, will produce synchrotron emission inside the GMC.

For the case of a weaker magnetic field, e.g.  $B_{\perp}=0.1 \text{ mG}$ , which is lower than appears to be present in the Sgr B2 GMC but which may occur in some other clouds, the Lorentz factor of electrons mainly responsible for emission at 1 GHz is  $\gamma_e \approx 1500$ , and more significant penetration of primary cosmic ray electrons would take place unless  $\chi \ll 1$ .

### 3.3 Predicted synchrotron emission from Sgr B2

At frequency  $\nu$ , for each point within the Sgr B2 giant molecular cloud complex we determine the  $H_2$  number density to find the synchrotron emission coefficient corresponding to complete penetration of cosmic rays within the cloud complex. Multiplying this by the cosmic ray penetration factor and  $f_{CR}$  we obtain the synchrotron emission coefficient  $j_{\nu}(\vec{r})$  taking account of cloud penetration and the possibility of cosmic ray enhancement in the Galactic Centre region compared to that locally. The synchrotron emission coefficient at 0.3 GHz is plotted as a function of distance from the centre of the Sgr B2 GMC for  $B_{\perp}=0.8 \text{ mG}$  and  $B_{\perp}=0.1 \text{ mG}$  in Fig. 7. In both cases, for  $\chi \leq 1$  the emission coefficient at the cloud complex centre is negligible compared to that near its edge.

We obtain the intensity  $I_{\nu}(\theta)$ , shown in Fig. 8 as a function of angular distance  $\theta$  for two frequencies, by integrating through the cloud complex assuming the synchrotron emission is optically thin,

$$I_{\nu}(\theta) = \int j_{\nu}(\vec{r}) d\ell.$$

Depending on the diffusive transport suppression factor  $\chi$ ,

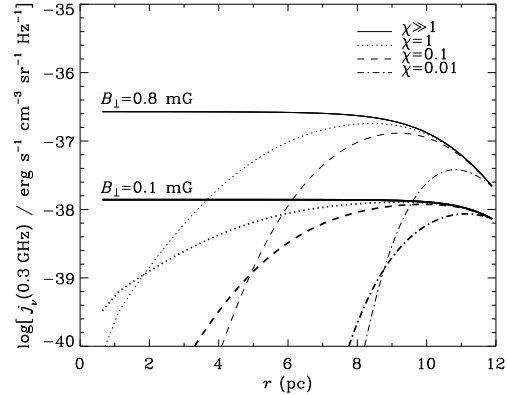


**Figure 7.** Emission coefficient at frequency  $\nu=0.3 \text{ GHz}$  vs. distance from the centre of the Sgr B2 GMC for  $B_{\perp}$  as indicated and for diffusion as defined by Eq 4 with  $\chi$  as labeled.

we may expect significant “limb brightening” of the synchrotron emission. We find that in the case of the Sgr B2 complex most of the flux comes from within  $\sim 11 \text{ pc}$  of its centre.

## 4 DISCUSSION

Radio continuum observations of the Sgr B2 GMC, including new measurements at 1.4 GHz and 2.4 GHz, are discussed in detail in a separate paper by Jones et al. (2008a). Since we want to compare the continuum emission in the Sgr B2 region with our predictions for the region of the dense central region of the giant molecular cloud we use continuum flux estimates for the region 11 pc in size centred midway between Sgr B2 (M) and Sgr B2 (N). Note that other papers may use quite different sizes for the Sgr B2 region and hence quote very different fluxes. In this complex region of the Galaxy, when assembling radio spectra from fluxes established by different groups, it is essential to use fluxes obtained over the same solid angle.

No evidence was found for diffuse, non-thermal emission out to  $\sim 11 \text{ pc}$  from the centre of the Sgr B2 GMC with limb-brightening as predicted for synchrotron emission by secondary electrons in the previous section, consistent with the results of Lang et al. (2008) who find a thermal spectrum for Sgr B2 including its envelope. Nor was there any suggestion of polarised emission characteristic of synchrotron emission. However, the major HII regions Sgr B2(M) and Sgr B2(N) showed up at all frequencies, and there is evidence of a strong non-thermal source to the south, which we have marked as “Non-Thermal Source” in Fig. 3, which is the subject of a separate paper ?. Figure 9 shows the spectral energy distribution for the central region of the Sgr B2 GMC (excluding the Non-Thermal Source), and therefore includes the combined fluxes from the major HII regions.

Sgr B2 is by far the most massive molecular cloud in the Galaxy and it is near the Galactic Centre which is almost certainly a region of enhanced cosmic rays. When selecting Sgr B2 for our study, we knew that separating out the thermal emission would be extremely difficult. Our search for



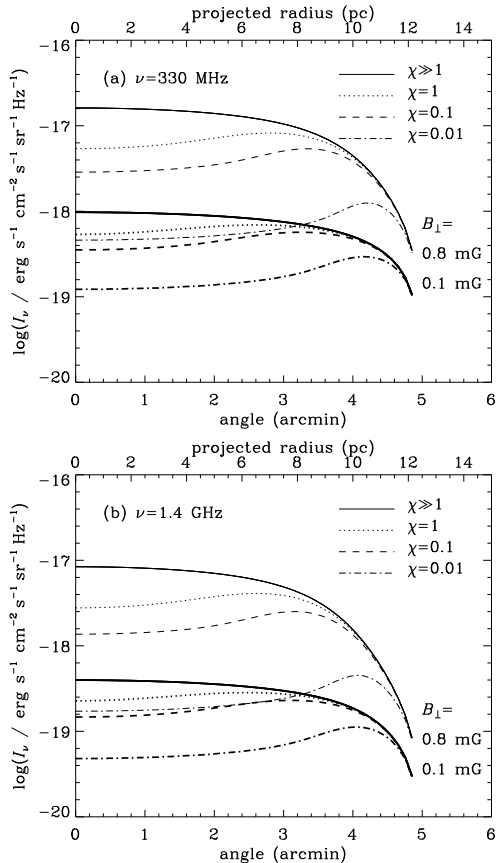


**Figure 8.** Predicted specific intensity  $I_\nu(\theta)$  at (a) 330 MHz, and (b) 1.4 GHz, as a function of angular distance from the centre of the Sgr B2 complex for diffusion as defined by Eq 4 with  $\chi$  as labeled, a cosmic ray flux equal to that at Earth and for magnetic field as labeled.

any comparable mass molecular cloud with no star formation was unsuccessful.

Before estimating upper limits to any synchrotron emission from secondary electrons in the Sgr B2 GMC, we shall attempt to fit the observed spectral energy distribution solely by thermal emission processes. A large number of UCHII regions have been observed at high frequencies, and so our first step will be to extrapolate their spectra to low frequencies. This will be done under the assumption that each known UCHII region is a homogeneous sphere of ionized interstellar gas, and we shall sum the contributions from all known UCHII regions. Clearly this will be an approximation as there will also be contributions from as-yet undiscovered UCHII regions, and because many of the UCHII regions will not be homogeneous, having density gradients, e.g. winds. We shall find that the UCHII regions account for  $\sim 50\%$  of the high frequency flux, and give a negligible fraction of the observed flux at low frequencies under these assumptions. The second step will be to fit the residual flux as thermal emission. The shape of the spectral energy distribution between 330 MHz and 1.4 GHz is suggestive of thermal emission from a region, or regions, with a density gradient, and we shall model it as a free-free emission from one, or many identical, single temperature winds. While this

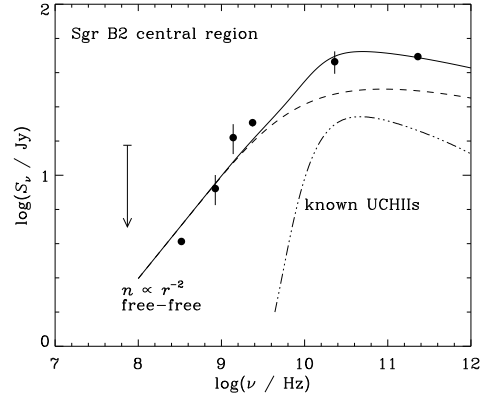


**Figure 9.** Observed fluxes summarized by Jones et al. (2008a) from the central region of Sgr B2 complex including the major HII regions but excluding the Southern Non-Thermal Source. The flux from the known UCHII regions is indicated (chain curve), and the best fitting model of free-free emission from a constant temperature spherical envelope or wind with  $n \propto r^{-2}$  is shown by the dashed curve, and the solid curve gives the sum of the two thermal components.

is clearly unrealistic, the data available to us do not justify a more sophisticated treatment.

#### 4.1 Free-free emission from UCHII regions

The emission at the higher frequencies (22 GHz and 43 GHz) is clearly thermal. Regions with very low emission measures and high 22 GHz and 43 GHz fluxes could potentially affect the emission at low frequencies. In order to investigate how much of the flux at these lower frequencies could be attributed to UCHII regions, we modeled the emission from the  $\sim 60$  known individual compact and UCHII regions reported in Gaume et al. (1995) and de Pree et al. (1998). This was achieved by “bootstrapping” the flux at the respective frequencies such that

$$S_\nu = \sum_k S_{\nu_i}^{(k)} \left( \frac{\nu}{\nu_i^{(k)}} \right)^2 \left( \frac{1 - e^{-\tau_\nu^{(k)}}}{1 - e^{-\tau_{\nu_i}^{(k)}}} \right)$$

where  $\nu_i = 22$  GHz or 43 GHz, the sum over the  $\sim 60$  UCHII regions with the label  $(k)$  relates to the  $k$ th UCHII region, and the frequency dependence of the thermal bremsstrahlung absorption coefficient is taken from Rybicki & Lightman (1979). The summed flux from the known UCHII regions has been added to Fig. 9, and it can be seen that the total flux from these regions accounts for about 50% of the 23 and 230 GHz flux but their contribution below 3 GHz is negligible.

#### 4.2 Free-free emission from envelopes or winds with density gradients

Between 330 MHz and 1.4 GHz the spectrum may be fitted with a single power-law  $S_\nu \sim \nu^{0.6}$  characteristic of optically thick emission from a spherical envelope or wind with a density gradient of the form

$$n_e(r) = n_i(r) = n_0 \left( \frac{r}{r_0} \right)^{-2}$$

as described by Panagia & Felli (1975) who give the expected flux at low frequencies

$$S_\nu^{\text{thick}} = 0.611 \left( \frac{n_0}{1 \text{ cm}^{-3}} \right)^{4/3} \left( \frac{r_0}{1 \text{ pc}} \right)^{8/3} \left( \frac{\nu}{10 \text{ GHz}} \right)^{0.6} \left( \frac{T}{10^4 \text{ K}} \right)^{0.1} \left( \frac{d}{1 \text{ kpc}} \right)^{-2}.$$

For the case of optically thin emission we can use

$$\int_{r_0}^{\infty} 4\pi r^2 n_e(r) n_i(r) dr = 4\pi n_0^2 r_0^3$$

together with the free-free emission coefficient and Gaunt factor  $g(T, \nu)$  from Rybicki & Lightman (1979) to obtain the flux at high frequencies where it is expected to be optically thin

$$S_\nu^{\text{thin}} = 1.6 \times 10^{-5} \left( \frac{n_0}{1 \text{ cm}^{-3}} \right)^2 \left( \frac{r_0}{1 \text{ pc}} \right)^3 \left( \frac{T}{10^4 \text{ K}} \right)^{-0.5} g(T, \nu) \left( \frac{d}{1 \text{ kpc}} \right)^{-2}.$$

Taking the optical depth to be  $\tau_\nu = S_\nu^{\text{thin}}/S_\nu^{\text{thick}}$  the flux from the envelope or wind is  $S_\nu = S_\nu^{\text{thick}}(1 - e^{-\tau_\nu})$ .

We fit this density-gradient model to the observed 330 MHz to 230 GHz fluxes (after subtracting the contributions of known UCHII regions as shown by chain curve in Fig. 9) and this is shown by the dashed curve in Fig. 9; the solid curve shows the sum of the two thermal components. For a temperature  $T = 10^4$  K the best fitting parameters are  $n_0 = 3.47 \times 10^7 \text{ cm}^{-3}$  and  $r_0 = 4.12 \times 10^{-3} \text{ pc}$ . The high density and small size would indicate that the emission is likely to have come from winds off, or excited by, young stars within the HII regions. If the flux is due to  $N$  separate identical objects, their wind parameters would be  $n_0 = 3.47 \times 10^7 \times N \text{ cm}^{-3}$  and  $r_0 = 4.12 \times 10^{-3}/N \text{ pc}$  in order to give the same total spectrum.

### 4.3 Synchrotron emission by secondary electrons

In Fig. 10 we re-plot the spectral energy distribution and show the flux predictions for the synchrotron emission from secondary electrons. Given that we have found no evidence of synchrotron emission from secondary electrons, and that the observed radio continuum emission is consistent with a thermal origin, we shall require that any flux of synchrotron emission from secondary electrons be well below the observed 330 MHz flux. For this, we shall somewhat arbitrarily adopt an upper limit of  $S_\nu=1$  Jy at 330 MHz for any non-thermal component.

Comparing the predicted synchrotron flux in Fig. 10(a) with our adopted limit, we find that for  $B_\perp=0.8$  mG and  $f_{CR}=1$ , the diffusion factor must be  $\chi < 0.02$ . With a significantly lower magnetic field such as  $B_\perp=0.1$  mG (see Fig. 10b), even  $\chi \gg 1$  (unimpeded cosmic ray penetration) is allowed and for this case cosmic ray enhancement in the Galactic Centre region at multi-GeV energies up to a factor  $f_{CR} < 2.5$  higher than in the Solar neighbourhood is not excluded. For this magnetic field, and more reasonable

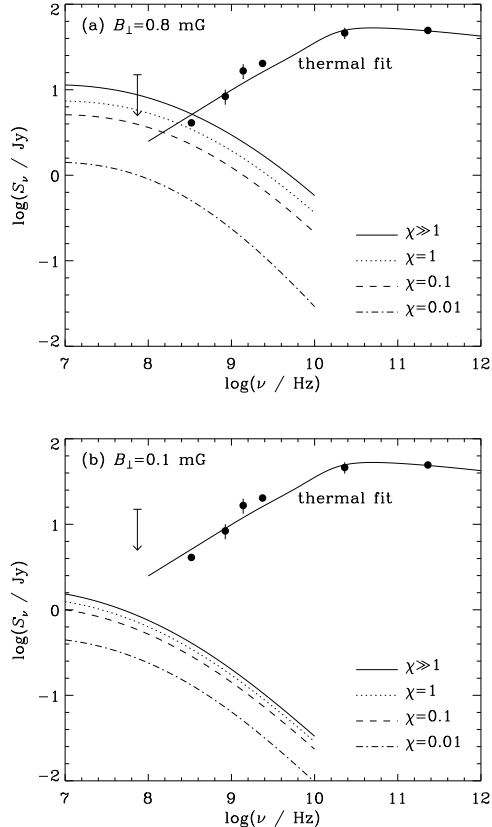


**Figure 10.** Observed fluxes summarized by Jones et al. (2008a) from the central region of Sgr B2 complex including the major HII regions but excluding the Southern Non-Thermal Source plotted together with fluxes predicted for (a)  $B_\perp = 0.8$  mG, (b)  $B_\perp = 0.1$  mG, and a cosmic ray spectrum as in the solar neighbourhood. Predicted fluxes are shown for diffusion as defined by Eq 4 with  $\chi$  as indicated. The total estimated thermal flux from the major HII regions is shown by the upper solid curve.

diffusion factors, the maximum allowed cosmic ray enhancement is 3 ( $\chi=1$ ), 3.9 ( $\chi=0.1$ ), 7.7 ( $\chi=0.01$ ). We emphasize that these are upper limits for cosmic ray enhancement and that there is no evidence for any cosmic ray enhancement at multi-GeV energies. In fact for the higher magnetic field, i.e.  $B_\perp=0.8$  mG, which is based on Zeeman splitting observations, the data suggest that there is no enhancement, or that cosmic rays at these low energies are unable to significantly penetrate into the Sgr B2 GMC.

In conclusion, we have no evidence that synchrotron emission by electrons and positrons produced by cosmic ray interactions has been observed from the Sgr B2 molecular cloud complex. The most likely explanation for this is that, for reasonable diffusion models, cosmic rays with multi-GeV energies (that produce secondary electrons with the right energy to radiate at GHz frequencies in  $\sim 0.8$  mG fields) cannot penetrate into the dense central regions of Sgr B2 GMC where much of the potential mass of target nuclei is located. This exclusion is also the likely explanation for non-observation of the Sgr B2 GMC by EGRET because it is again the same multi-GeV energy protons producing pions in  $pp$  collisions followed by  $\pi^0 \rightarrow \gamma\gamma$  that make an important

contribution to 100 MeV to multi-GeV gamma-rays. The observation of the Sgr B2 GMC by HESS (Aharonian et al. 2006) at TeV energies is consistent with more complete penetration of cosmic rays at higher energies into the dense central regions.

In choosing giant molecular clouds in the central region of the Galaxy for future investigation of their synchrotron emission by secondary electrons, one would look for a GMC with a mass of a few  $10^5 M_{\odot}$ , a lower central density than Sgr B2, e.g.  $n_{H_2} \sim 10^4 \text{ cm}^{-3}$  so that low energy cosmic rays may more easily penetrate it, a magnetic field above 0.1 mG and little star formation. We do not know of any, but such clouds may become apparent with the aid of new infrared surveys.

Finally, we emphasise that as we have no independent knowledge of the diffusion coefficient within the Sgr B2 GMC, i.e.  $\chi$  is unknown, we are unable to make a definitive statement about the enhancement of the low energy cosmic ray flux in the central region of the Galaxy relative to that in the Solar neighbourhood.

#### ACKNOWLEDGMENTS

The National Radio Astronomy Observatory is a facility of the National Science Foundation operated under cooperative agreement by Associated Universities, Inc. The Australia Telescope Compact Array is part of the Australia Telescope which is funded by the Commonwealth of Australia for operation as a National Facility managed by CSIRO. This research was supported under the Australian Research Council's Discovery Project funding scheme (project number DP0559991). While this research was conducted Professor R. D. Ekers was the recipient of an Australian Research Council Federation Fellowship (project number FF0345330). The authors thank T. Stanev for providing particle physics data employed in this paper. We thank the referee for helpful comments.

#### REFERENCES

Aharonian, F., et al, *Nature*, 2006, 439, 695.  
 Beakom, J.F., & Yüksel, H., 2006, *Phys. Rev. Lett.*, 97, 071102.  
 Beatty, J. J., et al., 2004. *Phys. Rev. Lett.* 93, 241102.  
 Brogan, C. L., Nord, M., Kassim, N., Lazio, J., & Anantharamaiah, K. 2003, *Astronomische Nachrichten Supplement*, 324, 17  
 Cesarsky, C. J., & Volk, H. J. 1978, *AAP*, 70, 367  
 Cheng, K. S., Chernyshov, D. O., & Dogiel, V. A. 2007, *AAP*, 473, 351  
 Crocker, R. M., Jones, D., Protheroe, R. J., Ott, J., Ekers, R., Melia, F., Stanev, T., & Green, A. 2007, *ApJ*, 666, 934  
 Crutcher, R.M., Roberts, D.A., Mehringer, D.M., Troland, T.H., 1996, *ApJ*, 462, L79.  
 Crutcher, R.M., 1999, *ApJ*, 520, 706.  
 de Pree, C. G., Goss, W. M., & Gaume, R. A. 1998, *ApJ*, 500, 847  
 Dogel', V. A., & Sharov, G. S. 1990, *AAP*, 229, 259

Fryer, C. L., Rockefeller, G., Hungerford, A., & Melia, F. 2006, *ApJ*, 638, 786  
 Gabici, S., Aharonian, F. A., & Blasi, P. 2007, *AP&SS*, 309, 365.  
 Gaume, R.A., Claussen, M.J., 1990, *ApJ*, 351, 538.  
 Gaume, R. A., Claussen, M. J., de Pree, C. G., Goss, W. M., & Mehringer, D. M., 1995, *ApJ*, 449, 663.  
 Goicoechea, J.R., Rodriguez-Fernandez, N.J. & Cernicharo, J., 2004, *ApJ*, 600: 214.  
 Gordon, M.A., Bekermann, U., Mezger, P.G., Zylka, R., et al., *AAP*, 1993, 280, 208.  
 Grimani, C. et al., 2002. *A&A*, 392, 287.  
 Jones, D., Crocker, J., Ott, J., R.M., Ekers, R.D., Protheroe, R.J., 2008, submitted.  
 Jones, D.I., Protheroe, R.J., Crocker, R.M., 2008b, *Publ. Astron. Soc. Australia*, in press. arXiv:0805.1966  
 Lang, C.C., Palmer, P, Goss, W.M., eprint arXiv:0801.2168  
 LaRosa, T.N., Brogan, C.L., Shore, S.N., Lazio T. J., Kassim N. E., Nord M. E., 2005, *ApJ* 626.  
 Lis, D. C., & Goldsmith, P. F. 1989, *ApJl*, 337, 704  
 Mayer-Hasselwander, H. A., et al. 1998, *AAP*, 335, 161  
 Moskalenko, I.V., and Strong, A.W., 1998, *ApJ*, 493, 694.  
 Murakami, H., Koyama, K., Sakano, M., Tsujimoto, M., & Maeda, Y. 2000, *ApJ*, 534, 283  
 Murakami, H., Koyama, K., & Maeda, Y. 2001, *ApJ*, 558, 687  
 Neronov, A., Chernyakova, M., Courvoisier, T.J.-L. & Walter, R., astro-ph/0506437.  
 Ott, J., Weiss, A., Staveley-Smith, L., & Henkel, C. 2006, *Bulletin of the American Astronomical Society*, 38, 920.  
 Panagia, N., & Felli, M., 1975, *AAP*, 39, 1.  
 Rybicki, George B. & Lightman, Alan P., 1979, "Radiative Processes in Astrophysics" (John Wiley & Sons: New York) .  
 Sato, F., Hasegawa T., Whiteoak J.B., Miyawaki R., 2000, *ApJ*, 535, 857.  
 Skilling, J., & Strong, A. W. 1976, *AAP*, 53, 253  
 Takagi, S., Murakami, H. & Koyama, K., 2002, *ApJ*, 573, 275.  
 Tsuboi M, 1999, *ApJS*, 120, 1.  
 van der Tak, F. F. S., Belloche, A., Schilke, P., Güsten, R., Philipp, S., Comito, C., Bergman, P., Nyman, L.-A., 2006, *A. & A.*, 454, L99  
 Weidenspointner, G., 2006, *A. & A.*, 450, 1013.  
 Yusef-Zadeh, F., Munro, M., Wardle, M., & Lis, D. C. 2007, *ApJ*, 656, 847